

Design optimization of wind turbine blades for reduction of airfoil self-noise[†]

Seunghoon Lee¹, Soogab Lee^{2,*}, Jaeha Ryi³ and Jong-Soo Choi³

¹Department of Mechanical and Aerospace Engineering, Seoul National University, Seoul, 151-744, Korea

²Engineering Research Institute, Department of Mechanical and Aerospace Engineering, Seoul National University, Seoul, 151-744, Korea

³Department of Aerospace Engineering, Chungnam National University, Daejeon, 305-764, Korea

(Manuscript Received May 31, 2012; Revised September 28, 2012; Accepted October 15, 2012)

Abstract

To reduce airfoil self-noise from a 10 kW wind turbine, we modified the airfoil shape and planform of a wind turbine blade. To obtain the optimal blade design, we used optimization techniques based on genetic algorithms. The optimized airfoil was first determined based on a section of the rotor blade, and then the optimized blade was designed with this airfoil. The airfoil self-noise from the rotor blades was predicted by using a semi-empirical model. The numerical analysis indicates that the level of the airfoil self-noise from the optimized blade is 2.3 dB lower than that from the baseline blade at the rated wind speed. A wind tunnel experiment was also performed to validate the design optimization. The baseline and optimized rotors were scaled down by a factor of 5.71 for the wind tunnel test. The experimental results showed that airfoil self-noise is reduced by up to 2.6 dB.

Keywords: Airfoil self-noise; Blade design; Design optimization; Noise reduction; Wind turbine

1. Introduction

Wind energy is one of the fastest-growing renewable energy resources. Although most wind turbines installed today are large, small wind turbines are also receiving attention because they can supply electricity in off-grid areas and can be installed close to a residence. However, because small wind turbines are generally installed in the vicinity of a dwelling, the noise from the wind turbine can annoy people who live in the surrounding area. Thus, reducing the noise of small wind turbines is important.

The aerodynamic noise generated from wind turbine blades, which is the dominant noise source of a typical wind turbine, is divided into two noise sources: turbulence ingestion noise and airfoil self-noise [1]. The turbulence ingestion noise is generated as the result of the interaction between atmospheric turbulence and the wind turbine blades, whereas the airfoil self-noise is generated without the existence of any atmospheric turbulence. The airfoil self-noise is composed of turbulent-boundary-layer trailing edge noise, laminar-boundary-layer vortex shedding noise, separation noise, and trailing edge bluntness noise [2]. Among these noise sources, the turbulent-boundary-layer trailing edge noise is the main noise source in typical operating conditions [3]. Accordingly, wind turbine noise can be reduced by controlling the turbulence

ingestion noise and the trailing edge noise.

However, because the turbulence ingestion noise has little relation to the shape of the wind turbine blade but is instead dependent on the inflow velocity and the turbulence characteristics, reducing the noise levels associated with it is difficult. On the other hand, the trailing edge noise can be reduced by altering the turbulent boundary layer structure or the trailing edge shape. For this reason, several attempts have been made to reduce the trailing edge noise by modifying the airfoil shape or attaching noise reduction materials to the blades [4–6]. However, most of these studies have focused on two-dimensional flow, and only a few studies have practically applied these techniques to the design of wind turbine blades [7, 8].

The purpose of this study is to reduce the airfoil self-noise generated from a 10 kW wind turbine rotor. In this study, the airfoil self-noise is reduced by modifying the airfoil shape and the blade planform, while the operating schedule and the rotor diameter remain fixed. To obtain the optimal designs of the airfoil shape and the blade planform, we use optimization methods that involve genetic algorithms. In designing our optimal blade, the optimized airfoil is first determined based on a section of the baseline blade. The optimal blade is then designed with this optimized airfoil.

2. Airfoil design optimization

2.1 Baseline wind turbine model

A 10 kW wind turbine was selected as the baseline wind

*Corresponding author. Tel.: +82 2 880 7384, Fax.: +82 2 876 4360

E-mail address: solee@snu.ac.kr

[†]Recommended by Associate Editor Do Hyung Lee

© KSME & Springer 2013

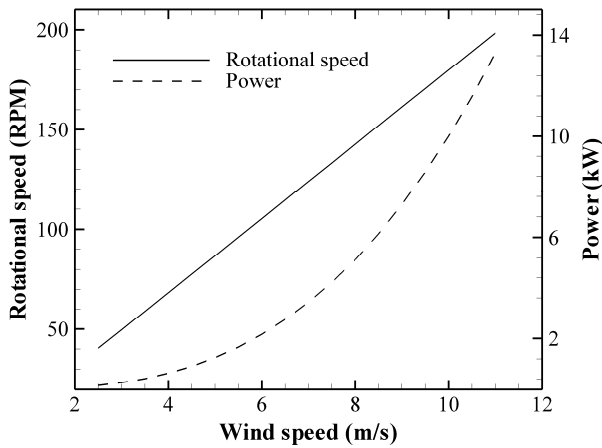


Fig. 1. Rotational speed and power output with respect to wind speed.

turbine. The baseline wind turbine is a three-bladed horizontal axis wind turbine. This turbine has a rotor diameter of 8 m and a hub height of 18 m. It reaches its rated rotational speed of 180 RPM at a wind speed of 10 m/s. Fig. 1 shows the rotational speed and the power output with respect to wind speed for this wind turbine.

2.2 Airfoil optimization procedure

To reduce airfoil self-noise generated from the wind turbine blades, the blade section was modified from that of the baseline blade by using an optimization method. Since airfoil self-noise is mainly generated in the outboard region of wind turbine blades, the outboard section should be redesigned for noise reduction. In this study, the blade section at $r/R = 0.75$ was selected as the baseline airfoil. To modify the baseline airfoil, shape functions were added linearly to the airfoil geometry by using the method proposed by Hicks and Henne [9]. A total of six shape functions, shown in Eq. (1), were applied to the upper and lower surfaces.

$$y = y_0 + \sum_{i=1}^6 X_i Y_i(x) \quad (1)$$

where

$$\begin{aligned} Y_1(x) &= x^{0.5} (1-x) e^{-15x} \\ Y_2(x) &= \sin^3(\pi x^{0.25}) \\ Y_3(x) &= \sin^3(\pi x^{0.757}) \\ Y_4(x) &= \sin^3(\pi x^{1.357}) \\ Y_5(x) &= x^{0.5} (1-x) e^{-10x} \\ Y_6(x) &= \sin^3\{\pi(1-x)^{0.32}\}. \end{aligned}$$

In Eq. (1), X_i and Y_i are the shape function coefficients and

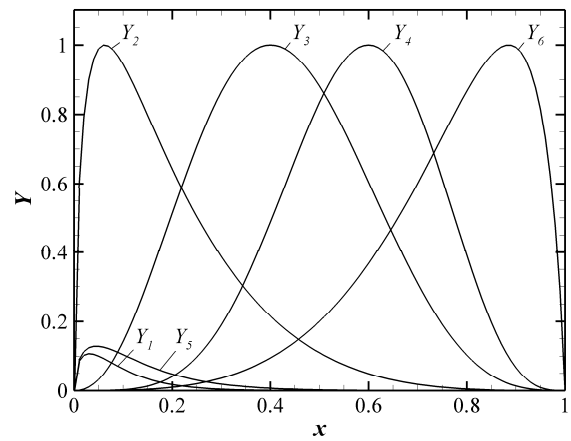


Fig. 2. Airfoil shape functions.

shape functions, respectively. The six shape functions are plotted in Fig. 2.

A multi-island genetic algorithm was used to determine the optimal values of the shape function coefficients [10]. The objective function for the optimization was defined as the overall sound pressure level of the trailing edge noise because previous studies showed that it is the main noise source of wind turbine noise [3]. The Reynolds number, Mach number, and angle of attack used in the calculation were $Re = 1.32 \times 10^6$, $M = 0.167$, and $\alpha = 4^\circ$, respectively. These values correspond to the aerodynamic conditions of the blade section at $r/R = 0.75$ for the rated wind speed. In addition, the span and chord length used in the calculation were 3.6 m and 0.3423 m, respectively; the chord length is identical to that of the blade section at $r = 0.75R$. The observer was located upwards from the trailing edge, and the distance from the trailing edge to the observer was 3 m.

A semi-empirical model proposed by Brooks, Pope, and Marcolini [2] was used to predict the overall sound pressure level of the trailing edge noise. They performed extensive wind tunnel experiments to measure airfoil self-noise from NACA0012 airfoil models. The semi-empirical model was developed based on the results of these experiments. According to [2], the one-third octave band sound pressure level (SPL) of trailing edge noise can be described by

$$SPL_{TEN} = 10 \log \left(10^{SPL_\alpha/10} + 10^{SPL_s/10} + 10^{SPL_p/10} \right) \quad (2)$$

where

$$\begin{aligned} SPL_p &= 10 \log \left(\frac{\delta_p^* M^5 \bar{ID}}{r_e^2} \right) + A \left(\frac{St_p}{St_1} \right) + (K_1 - 3) + \Delta K_1 \\ SPL_s &= 10 \log \left(\frac{\delta_s^* M^5 \bar{ID}}{r_e^2} \right) + A \left(\frac{St_s}{St_1} \right) + (K_1 - 3) \\ SPL_\alpha &= 10 \log \left(\frac{\delta_s^* M^5 \bar{ID}}{r_e^2} \right) + B \left(\frac{St_s}{St_2} \right) + K_2. \end{aligned}$$

In Eq. (2), δ^* , St , l , \bar{D} indicate the boundary layer displacement thickness, Strouhal number, wing span, and stream-wise noise directivity, respectively. The subscripts p , s , and α represent the pressure side, suction side, and nonzero angle of the attack effect, respectively. Functions A and B define the spectral shapes of the trailing edge noise. St_1 and St_2 are the peak Strouhal numbers where the trailing edge noise is maximum. K_1 , K_2 , and ΔK_1 are empirical constants to adjust the level of trailing edge noise. The definitions of the spectral curves, the peak Strouhal numbers, and the empirical constants are described in Ref. [2].

For the directivity function, this model uses a cardioid-type directivity pattern, which is the theoretical directivity for a semi-infinite flat plate. This directivity is based on the assumption that the chord length is much larger than the dominant acoustic wavelength, which was not satisfied in the present calculation. However, in the present case, the noise was predicted for an observer normal to the airfoil chord. Accordingly, the results would be unaffected by this directivity; the directivity function simply equals one.

The displacement thicknesses of the suction and pressure side boundary layers in Eq. (2) were calculated by using XFOIL code [11]. The angle of attack used for the calculation of boundary layer displacement thickness was based on the aerodynamic angle of attack at a zero lift angle.

Although the sound pressure level of the airfoil self-noise was reduced by using the optimization procedure, the aerodynamic performance of the modified blade should not be worse than that of the baseline blade. In this optimization procedure, a constraint condition was chosen to not only maintain but also enhance the aerodynamic performance of the optimized airfoil; this condition is shown in Eq. (3).

$$L/D_{\text{optimized}, \alpha=4^\circ} > L/D_{\text{baseline}, \alpha=4^\circ} \times 160\% \quad (3)$$

where L and D are the lift and drag of the airfoil, respectively. The XFOIL code was again used to calculate aerodynamic properties such as lift and drag coefficients [11].

Moreover, the maximum thickness of the modified airfoil, t_{max} was also subject to a constraint. If the maximum thickness of the optimized airfoil was thicker than that of the baseline airfoil, the possibility of an increase in the blade weight exists. On the other hand, if the maximum thickness was thinner than the baseline, a structural problem may arise in the inboard region. Thus, the constraint condition in this optimization procedure was chosen, as shown in Eq. (4).

$$-5\% < \frac{t_{\text{max}} - t_{\text{max, baseline}}}{t_{\text{max, baseline}}} < 5\% \quad (4)$$

Although the object function was defined as the level of the trailing edge noise, the trailing edge bluntness noise was also calculated to evaluate the airfoil self-noise of the baseline and optimized airfoils. The trailing edge bluntness noise was pre-

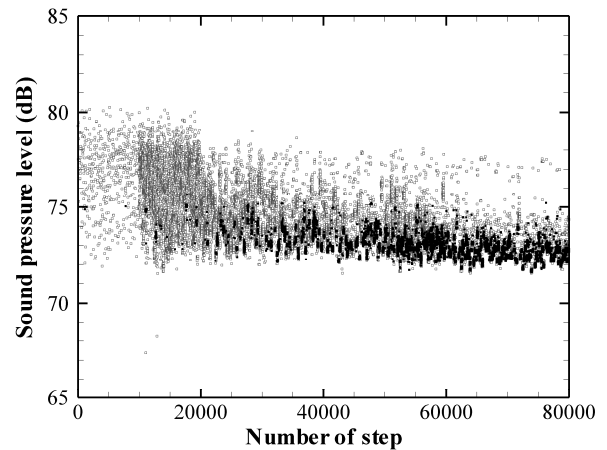


Fig. 3. Calculated sound pressure level of modified airfoil during the optimization; black indicates runs that satisfy the constraint conditions; gray indicates runs that did not satisfy the constraint conditions.

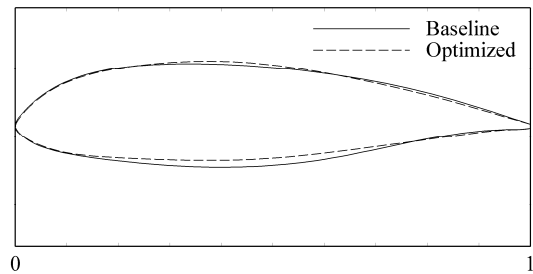


Fig. 4. Geometries of the baseline and the optimized airfoils.

dicted by the same model proposed by Brooks, Pope, and Marcolini [2]. The trailing edge thickness normalized by the chord length was 0.0082, and the flow angle was 22° , which is the solid angle of the airfoil surface near the trailing edge.

2.3 Airfoil optimization result

A total of 80000 runs were carried out. Calculated sound pressure levels during the optimization procedure are presented in Fig. 3. The optimum design was obtained in the 73851th run.

Fig. 4 presents the geometry of the baseline and optimized airfoils. The maximum thickness was decreased from 21.6% to 20.8% in the optimized airfoil. The trailing edge thickness and solid angle at the trailing edge changed little after the optimization. Notably, the gradient of the airfoil shape was reduced in the vicinity of the trailing edge.

The overall sound pressure levels of the airfoil self-noise with respect to the angle of attack for the baseline and optimized airfoils are shown in Fig. 5. The result indicates that the optimized airfoil generated less noise than the baseline airfoil at positive angles of attack. The noise reduction of 3.3 dB was achieved at an angle of 4° , which was the target angle for the optimization. The reason for the noise reduction may be that the decrease of the gradient near the trailing edge leads to a

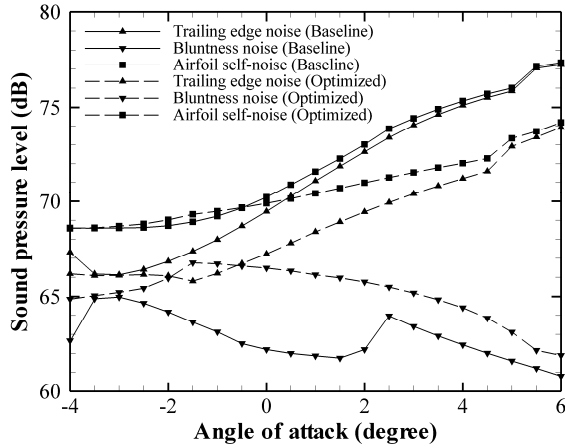


Fig. 5. Overall sound pressure levels of the airfoil self-noise for the baseline and optimized airfoil. The airfoil self-noise is the sum of the trailing edge noise and trailing edge bluntness noise.

decrease in the boundary layer displacement thickness.

Moreover, although trailing edge noise was the dominant noise source of the airfoil self-noise, the trailing edge bluntness noise level became comparable to that of the trailing edge noise at negative angles of attack. This condition occurs because the boundary layer is thin at a low angle of attack, which leads to a high ratio of trailing edge thickness to boundary layer displacement thickness. The airfoil self-noise from the optimized airfoil was higher than that from the baseline airfoil at negative angles of attack due to the high level of the trailing edge bluntness noise. However, this noise increase would not be a problem because the angle of attack of wind turbine blades is positive in typical operating conditions.

3. Blade design optimization

3.1 Blade optimization procedure

In the blade design procedure, the optimized airfoil obtained from the previous section was identically applied to all the blade sections. The blade planform was then optimized to obtain the blade that generates the least airfoil self-noise. The chord length distribution along the blade span was modeled as a linear function, as seen in Eq. (5).

$$c = c_1 \times (r - r_{\text{cut}}) / R + c_2 \quad (5)$$

where r_{cut} is the distance between the hub cutout and the rotor center, and R is the rotor radius. The twist distribution along the blade span was modeled to be inversely proportional to the blade radius, as shown in Eq. (6).

$$t = t_1 \times (r/R)^{-t_2} + t_3 \quad (6)$$

Thus, a total of five variables (c_1 , c_2 , t_1 , t_2 , and t_3) were used in the optimization procedure.

To design an optimized blade which has a low noise level in a range of wind speeds, the overall sound pressure levels of the trailing edge noise at wind speeds of 7 m/s and 10 m/s were chosen as the objective functions. The optimization problem had two objective functions, so the neighborhood cultivation genetic algorithm, which is effective for optimization problems with more than one objective function, was used in this optimization procedure [12].

The trailing edge noise generated from the wind turbine blades was predicted at a reference position according to IEC 61400-11 standard [13]. The reference position was located in a downwind direction at a distance equal to the sum of the hub height and rotor radius. For the prediction of the trailing edge noise, each blade was divided into 20 equally spaced segments. The semi-empirical model used in the previous section was then applied to each blade segment. One-third octave band spectra were obtained by summing up all the noise spectra of the blade segments with respect to retarded time. The inflow wind speed and the effective angle of attack at each blade segment, which is necessary for the prediction of the trailing edge noise, were calculated by using an in-house program which employed the blade element momentum theory.

Three constraints were imposed in the optimization procedure. First, to maintain the wind turbine performance in all ranges of wind speeds, power outputs at wind speeds of 2.5, 4, 7, and 10 m/s were selected as constraints. In this study, to enhance the wind turbine performance, the constraint conditions were set as in Eqs. (7a) to (7d).

$$P_{2.5\text{m/s}} > P_{2.5\text{m/s, baseline}} \times 103\% \quad (7a)$$

$$P_{4\text{m/s}} > P_{4\text{m/s, baseline}} \times 105\% \quad (7b)$$

$$P_{7\text{m/s}} > P_{7\text{m/s, baseline}} \times 105\% \quad (7c)$$

$$P_{10\text{m/s}} > P_{10\text{m/s, baseline}} \times 105\% \quad (7d)$$

where P is the rotor power. Furthermore, to avoid increasing the blade weight or applied load to the blade root, the chord length and the solidity were selected as constraints, as shown in Eqs. (8) and (9).

$$c_{\text{root}} > c_{\text{root, baseline}} \quad (8)$$

$$\sigma_{\text{baseline}} \times 95\% < \sigma < \sigma_{\text{baseline}} \quad (9)$$

3.2 Blade optimization result

A total of 20000 runs were carried out. The level differences of trailing edge noise between the baseline and modified blades during the optimization procedure are plotted in Fig. 6. The optimum design was obtained in the 13958th run.

Fig. 7 shows the chord and twist distributions for the baseline and optimized blades. The twist angle for the optimized blade was increased from that for the baseline blade. The chord length at the root was slightly longer than that of the baseline blade, whereas the chord length at the blade tip was

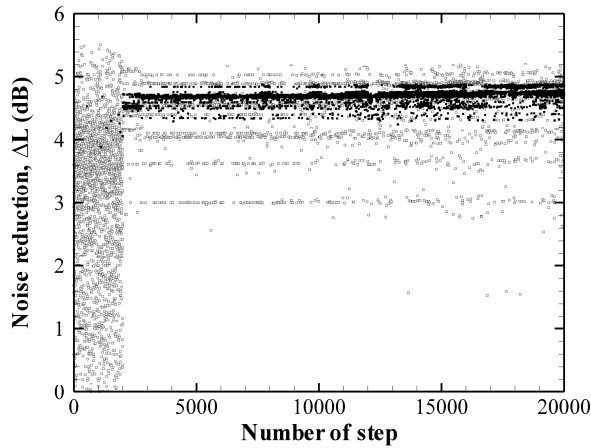


Fig. 6. Noise level difference between the baseline and modified blades, $\Delta L = SPL_{\text{baseline},10\text{m/s}} - SPL_{\text{modified},10\text{m/s}} + SPL_{\text{baseline},7\text{m/s}} - SPL_{\text{modified},7\text{m/s}}$; black indicates runs that satisfy the optimization constraints; gray indicates runs that did not satisfy the optimization constraints.

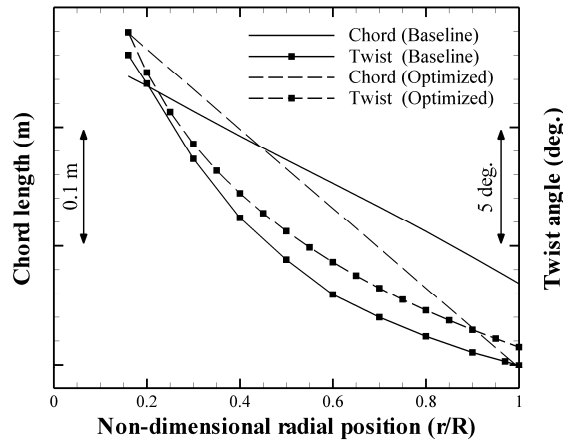


Fig. 7. Chord and twist distributions for the baseline and optimized blades.

shorter than that of the baseline blade.

The numerical predictions of the overall sound pressure level for the baseline and optimized wind turbines are plotted in Fig. 8. These predictions include not only trailing edge noise but also trailing edge bluntness noise. The result indicates that the optimized wind turbine generated less noise than the baseline wind turbine at most wind speeds. The airfoil self-noise was reduced by 2.3 dB at a wind speed of 10 m/s. At wind speeds less than 5 m/s, little difference was observed between the noise levels of the baseline and optimized blades. However, in this range of wind speeds, the noise level of the airfoil self-noise is small compared with that of typical background noise. Thus, airfoil self-noise reduction at low wind speeds is unnecessary in most situations.

In addition, the prediction results show that the trailing edge bluntness noise is negligible compared with the trailing edge noise. However, for the optimized blade, the contribution of the bluntness noise to the overall noise increased as the wind speed increased.

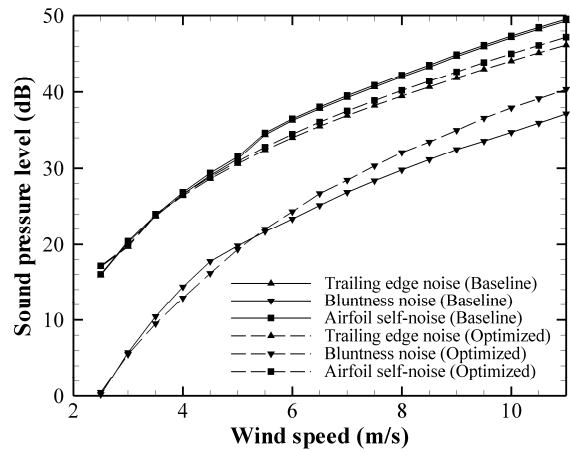


Fig. 8. Predicted overall sound pressure levels for the baseline and optimized wind turbines. The airfoil self-noise is the sum of the trailing edge noise and the trailing edge bluntness noise.

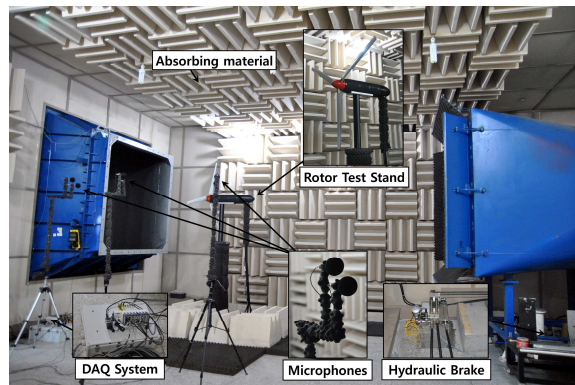


Fig. 9. Configuration for the small-scale wind turbine rotor test stand in the anechoic wind tunnel.

4. Experiments

4.1 Experiment apparatus

A wind tunnel experiment was performed to validate the result of the design optimization. The experiment was carried out in a semi-anechoic wind tunnel at Chungnam National University. Fig. 9 shows a photograph of the wind tunnel test system and the semi-anechoic chamber. The wind tunnel has a cross section of 1.8 m × 1.8 m and is capable of generating wind speeds of up to 35 m/s. The anechoic chamber has a total volume of 211.9 m³ and a cut-off frequency of 150 Hz, which is far below the frequency of typical airfoil self-noise.

To evaluate the turbulence characteristics of the wind tunnel, the turbulence intensity for the wind tunnel was measured by using hot-wire anemometry. The measurement system was composed of a hot-wire anemometry system (A.A.Lab.System AN-1003) with a hot-wire probe (Dantec 55R01). The turbulence intensity was measured at velocities of up to 30 m/s. The measurement results are presented in Table 1.

A test system for measuring wind turbine rotor performance was developed and used in this experiment. The rotor per-

Table 1. Turbulence intensity with respect to inflow velocity.

Inflow velocity (m/s)	Turbulence intensity (%)	Inflow velocity (m/s)	Turbulence intensity (%)
5	0.3853	20	0.2722
10	0.3181	25	0.2705
15	0.3275	30	0.2563

formance was recorded by using a PC-based data acquisition system. The experimental data was measured by using the LabVIEW7.1™ software. In the rotor test stand, a rotating balance that consists of a full-bridge strain gage was installed to measure the thrust and the hub moment. The rotor test stand was overspread with a windshield along the direction of the slipstream to minimize the interaction between the shear layer with the supporting structure. A pitot tube was used to measure the wind tunnel velocity. Air temperature, air pressure, and humidity were also recorded during the experiment.

The baseline and optimized rotors were scaled down by a factor of 5.71 for the wind tunnel test. The small-scale rotors had a diameter of 1.4 m, and their rotational speeds ranged from 491 RPM to 1473 RPM. By increasing the rotational speed of the small-scale rotor, the tip speed of the model blades was set to be equal to that of the full-size 10 kW wind turbine blades. Since the disk area of the small-scale rotors was smaller than the cross section of the wind tunnel, the interaction between the rotor blades and shear layer turbulence was expected to be negligible.

For the measurement of trailing edge noise, the boundary layers were tripped with dotted strips to ensure that the boundary layers on the blades were fully turbulent. The height of the dotted strip was determined by using the method proposed by Alfredsson and Dahlberg [14]. The ratio of particle height to the transition position can be described as Eq. (10).

$$\frac{k}{x} = \left[(\text{Re}_x)^{-3/2} \frac{R_k}{0.3172} \right]^{1/2} \quad (10)$$

where R_k is the particle Reynolds number, and x is the transition position where the dotted strips were attached. The particle Reynolds number of 600 was selected in this experiment. The dotted strips were attached at 10% chord from the leading edge. Fig. 10 presents the small-scale blade with the dotted strips.

A total of six piezoelectric microphones (MG M360, 1/4" free-field type) were used for noise measurements. The microphones were calibrated at 1 kHz to 94 dB with an accuracy of ± 0.05 dB. They were located at distances of 2100 mm and 2,180 mm. Two of the microphones were placed in the rotating plane, while the other four microphones were placed near the rotating plane at an offset of 30°. The acoustic signals were acquired simultaneously by using an analog-to-digital (A/D) converter (NI PCI-4472) installed in a personal computer. The acoustic signals were recorded at a sampling frequency of 100 kHz with a duration of 20 seconds. Anti-aliasing filter was not used because the sampling frequency



Fig. 10. Small-scale blade and trip strip on the blade surface.

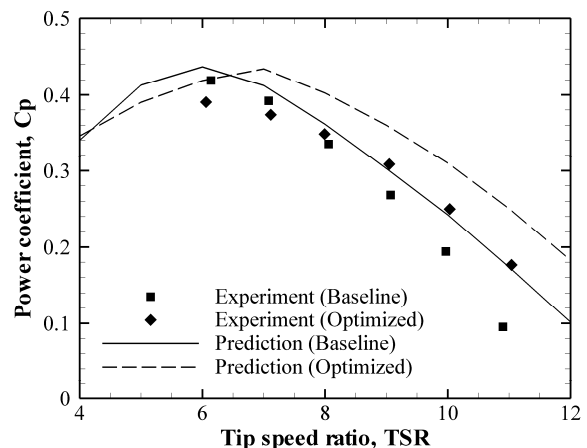


Fig. 11. Comparison of power coefficients between the experimental data and prediction results.

was much higher than the audible range of frequency. Moreover, a trigger signal was created by a photo sensor which was installed at the wind turbine rotating shaft. This signal was also recorded in the computer via the A/D converter.

4.2 Experiment result

Fig. 11 compares the measured and predicted power coefficients with respect to tip speed ratio. During the measurements, the wind speed was constant at 9 m/s. An offset was found between the measured and predicted results. This error is possibly due to the mechanical losses in the rotor hub, which was not considered in the numerical predictions. Furthermore, the numerical results indicate that the power output of the optimized blade was higher than that of the baseline blade in the rated operating condition, which is at a tip speed ratio of about 7.5. However, little difference between the power coefficients of the baseline and optimized blade was observed in the experimental results.

Fig. 12 shows the overall sound pressure level of the wind turbine noise with respect to tip speed ratio. The airfoil self-noise was reduced by up to 2.6 dB due to the design optimiza-

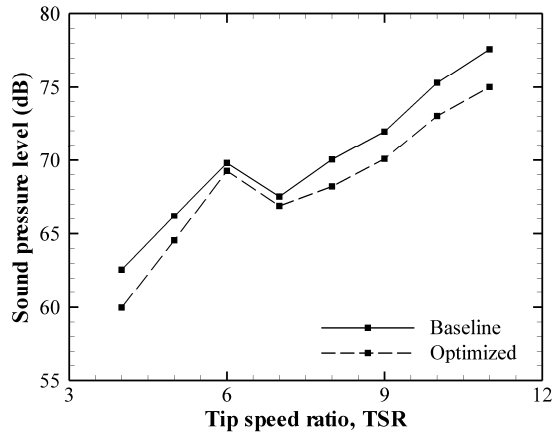


Fig. 12. Measured overall sound pressure levels for the baseline and optimized wind turbines.

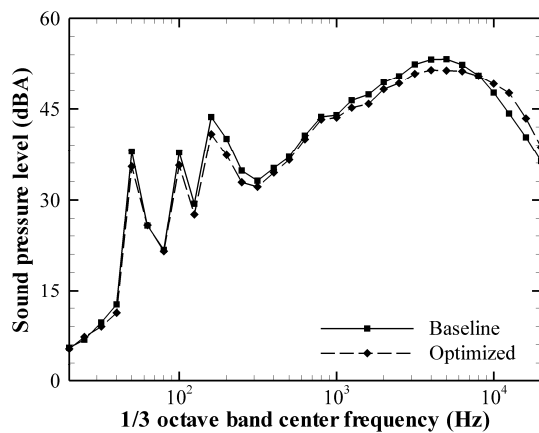


Fig. 13. Measured 1/3 octave band spectra for the baseline and optimized wind turbines.

tion. The A-weighted one-third octave band spectra for the baseline and optimized blade are shown in Fig. 13, which were measured at a tip speed ratio of 8. The large hump centered at about 4.5 kHz is the noise source due to trailing edge noise. This hump decreased as a result of the modification of the blade shape.

In addition, the broadband noise spectrum for the full-scale rotor can be estimated by using the result of the small-scale rotor tests. The peak frequency of trailing edge noise corresponds to the peak Strouhal number, which is mainly related to the Mach number and the angle of attack [2]. Since the tip Mach number for the small-scale rotor matched that for the full-scale rotor, the peak Strouhal number for the small-scale rotor would be the same as that for the full-scale rotor. From a simple calculation of boundary layer displacement thickness using an empirical equation [2], the boundary layer displacement thicknesses normalized by the chord length for the full-scale rotor were estimated to be about 1.65 times smaller than those for the small-scale rotor. Considering that the chord length for the full-scale rotor is 5.71 times larger than that for the small-scale rotor, the peak frequency for the full-scale

rotor would be about 1.3 kHz.

5. Conclusions

To reduce airfoil self-noise from a 10 kW wind turbine, we modified the airfoil shape and the planform of the wind turbine blade by using optimization techniques. In the optimization process, the airfoil shape was first modified, and then the blade planform was designed based on this optimized airfoil. The results of the numerical predictions showed that the sound level of the airfoil self-noise from the optimized blade was 2.3 dB lower than that from the baseline blade at a wind speed of 10 m/s. Moreover, a wind tunnel experiment was performed to validate the results of the design optimization. The results indicate that the airfoil self-noise generated from the wind turbine was reduced by up to 2.6 dB even though the aerodynamic performance remained the same as that of the baseline wind turbine. This optimization procedure could be utilized for any wind turbine when reducing aerodynamic noise is necessary.

Acknowledgment

This work was supported by the Human Resources Development Program (No. 20104010100490) of the Korea Institute of Energy Technology Evaluation and Planning (KETEP) grant funded by the Ministry of Knowledge Economy of the Korean government. This research was also supported by the Institute of Advanced Aerospace Technology at Seoul National University.

Nomenclature

A	: Spectrum function for trailing edge noise
B	: Spectrum function for angle-dependent trailing edge noise
c	: Chord length distribution (m)
c_{root}	: Chord length at the root (m)
\bar{D}	: Directivity function
k	: Particle height (m)
L/D	: Lift-to-drag ratio
l	: Span (m)
M	: Mach number
P	: Rotor power (kW)
R	: Rotor radius (m)
r	: Radial distance from rotor center (m)
r_{cut}	: Distance between hub cutout and rotor center (m)
Re	: Reynolds number
r_e	: Distance from source to observer (m)
R_k	: Particle Reynolds number
St	: Strouhal number
t	: Twist distribution (degree)
t_{max}	: Maximum thickness of airfoil (%)
X_i	: Shape function coefficients
Y_i	: Shape functions
α	: Angle of attack (degree)

δ^* : Boundary layer displacement thickness (m)
 σ : Blade solidity

References

- [1] S. Wagner, R. Bareiß and G. Guidati, *Wind turbine noise*, Springer, Berlin, Germany (1996).
- [2] T. F. Brooks, D. S. Pope and M. A. Marcolini, *Airfoil self-noise and prediction*, NASA Reference Publication 1218 (1989).
- [3] S. Oerlemans, P. Sijtsma and B. Méndez López, Location and quantification of noise sources on a wind turbine, *Journal of Sound and Vibration*, 299 (4-5) (2007) 869-883.
- [4] M. S. Howe, Noise produced by a sawtooth trailing edge, *Journal of the Acoustical Society of America*, 90 (1) (1991) 482-487.
- [5] F. Bertagnolio, H. Aa. Madsen and C. Bak, Trailing edge noise model validation and application to airfoil optimization, *Journal of Solar Energy Engineering*, 132 (3) (2010) 031010.
- [6] M. Herr and W. Dobrzynski, Experimental investigations in low-noise trailing-edge design, *ALAA Journal*, 43 (6) (2005) 1167-1175.
- [7] S. Oerlemans, M. Fisher, T. Maeder and K. Kögler, Reduction of wind turbine noise using optimized airfoils and trailing-edge serrations, *ALAA Journal*, 47 (6) (2009) 1470-1481.
- [8] S. Lee, S. Lee, B. Hwang and S. Lee, Blade optimization design of 10kW wind turbine for reduction of airfoil-self noise, *Proc. of the Korea Wind Energy Association 2010 Autumn Conference*, Changwon, Korea (2010) 103-106.
- [9] R. M. Hicks and P. A. Henne, Wing design by numerical optimization, *Journal of Aircraft*, 15 (7) (1978) 407-412.
- [10] R. Tanese, Distributed genetic algorithms, *Proc. of the 3rd International Conference on Genetic Algorithms*, Fairfax, Virginia, USA (1989) 434-439.
- [11] <http://web.mit.edu/drela/Public/web/xfoil> (Accessed 27 September 2012).
- [12] S. Watanabe, T. Hiroyasu and M. Miki, Neighborhood cultivation genetic algorithm for multi-objective optimization problems, *Proc. of the Genetic and Evolutionary Computation Conference*, New York, NY, USA (2002) 458-465.
- [13] IEC 61400-11:2002, Wind turbine generator systems - Part 11: Acoustic noise measurement techniques (2002).
- [14] P. H. Alfredsson, J. Å. Dahlberg, A preliminary wind tunnel study of windmill wake dispersion in various flow conditions, FFA Technical Note AU-1499, Part 7, Stockholm, Sweden (1979).



Seunghoon Lee is currently a Ph.D. candidate in the Department of Mechanical and Aerospace Engineering at Seoul National University. He received his M.S. and B.S. degrees from the School of Mechanical and Aerospace Engineering at Seoul National University in 2009 and 2007, respectively. His research interests include trailing edge noise generated from wind turbine blades, annoyance caused by wind turbine noise, and helicopter aerodynamics.



Soogab Lee is a professor in the Department of Mechanical and Aerospace Engineering at Seoul National University. He received his Ph.D. degree in Aeronautics and Astronautics from Stanford University in 1992. He worked as a research scientist at NASA Ames Research Center from 1992 to 1995. His research interests are in the area of aerodynamics and acoustics of rotating machines including wind turbine systems.



Jaeha Ryi is currently a Ph.D. candidate in the Department of Aerospace Engineering at Chungnam National University. He received his M.S. and B.S. degrees from the Department of Aerospace Engineering at Chungnam National University in 2008 and 2006, respectively. His research interests are in the experimental aerodynamics of rotating machinery including wind tunnel testing techniques, acoustics experiments of rotating machinery, and wind turbine blades.



Jong-Soo Choi is a professor in the Department of Aerospace Engineering at Chung-Nam National University. He received his Ph.D. degree in Aerospace Engineering from Pennsylvania State University (USA) in 1991. His research interests are in the experimental aerodynamics by wind tunnel testing, acoustics experiments of the mechanics of flow-induced sound, and noise visualization techniques including signal processing.